

Structural and optical properties of TiO₂ nanoparticles and their photocatalytic behavior under visible light

Propiedades estructurales y ópticas de las nanopartículas de TiO₂ y su comportamiento fotocatalítico bajo luz visible

Edgar Mosquera-Vargas^{1§}, Daniela Herrera-Molina¹, Jesús E. Diosa¹

¹Universidad del Valle, Facultad de Ciencias Naturales y Exactas, Departamento de Física & Centro de Excelencia en Nuevos Materiales, Grupo de Transiciones de Fase y Materiales Funcionales, Cali, Colombia

§edgar.mosquera@correounivalle.edu.co, daniela.herrera.molina@correounivalle.edu.co, jesus.diosa@correounivalle.edu.co

Recibido: 23 de enero de 2021 – **Aceptado:** 28 de abril de 2021

Abstract

TiO₂ nanoparticles were synthesized using a facile, reproducible, and scalable sol-gel method and their structural and optical properties was studied. XRD and FTIR was used to identify the phase, crystallite size, and functional groups present in the nanoparticles. The prepared samples crystallize in the anatase structure with a highly crystalline order. TEM/EDX shows that the nanoparticles are pure, spherical, and with an average particle size of 15 ± 2 nm. The optical band gap energy is around 3.69 ± 0.10 eV and exhibits blueshift with respect to the bulk anatase. PL emission is attributed to oxygen vacancies (Vo). All samples were photoactive for MO degradation after 240 min of being irradiated with visible light.

Keywords: Photocatalytic, Sol-gel synthesis, Structural and optical properties, TiO₂ nanoparticles.

Resumen

Nanopartículas de TiO₂ fueron sintetizadas utilizando un fácil, reproducible, y escalable método sol-gel y sus propiedades estructurales y ópticas estudiadas. Se usó XRD y FTIR para identificar la fase, el tamaño del cristalito y los grupos funcionales presentes en las nanopartículas. Las muestras preparadas cristalizan en la estructura anatasa con un orden altamente cristalino. TEM/EDX muestran que las nanopartículas son puras, esféricas y con un tamaño medio de partícula de 15 ± 2 nm. La energía de la banda prohibida óptica es de alrededor 3.69 ± 0.10 eV y presenta un desplazamiento hacia el azul con respecto a la anatasa en granel. La emisión de FL se atribuye a las vacantes de oxígeno (Vo). Todas las muestras fueron fotoactivas para la degradación de MO después de 240 min de ser irradiadas con luz visible.

Palabras claves: Actividad fotocatalítica, Nanopartículas de TiO₂, Propiedades estructurales y ópticas, Síntesis sol-gel.

Como citar:

Mosquera-Vargas E, Herrera-Molina D, Diosa JE. Propiedades estructurales y ópticas de las nanopartículas de TiO₂ y su comportamiento fotocatalítico bajo luz visible. INGENIERÍA Y COMPETITIVIDAD. 2021;23(2):e213e10965. <https://doi.org/10.25100/iyv.v23i2.10965>.



Este trabajo está licenciado bajo una Licencia Internacional Creative Commons Reconocimiento–NoComercial–CompartirIgual 4.0

1. Introduction

In the last few years, a large amount of environmental pollution and wastewater contamination, mainly due to dyes and toxic metal ions, have been continuously discharged into the atmosphere and effluents causing serious harm to human health and water reservoirs⁽¹⁻³⁾. Therefore, advanced oxidation processes (AOPs) such as heterogeneous photocatalysis could be a promising method for the degradation of various organic pollutants in wastewater⁽¹⁻¹⁰⁾.

Metal oxides-based semiconductors like ZnO and TiO₂ have been the most studied photocatalysts for oxidation of organic contaminants in wastewaters⁽¹⁻⁹⁾. Together with ZnO, TiO₂ is an effective and very well-known semiconductor with interesting optical and electrical properties^(2,9). In nature, the TiO₂ exists in different phases: rutile and anatase with tetragonal structure, and brookite with orthorhombic structure, being anatase the phase most attractive for a photocatalytic activity⁽¹¹⁾.

However, a new phase known as TiO₂(B) with monoclinic structure (considered as a metastable phase) has been previously reported⁽¹¹⁻¹⁴⁾. In addition, mixed TiO₂ (e.g. Ag/Co/Mn–TiO₂^(6,7,19), TiO₂/SnO₂⁽⁸⁾, TiO₂/CS⁽¹⁰⁾, CuO/CeO₂–TiO₂⁽³³⁾) has been widely used and studied as active catalyst for photodegradation of organics pollutants. However, TiO₂ is active under ultraviolet light (UV), and it is inactive in the visible region due to its wide band gap (E_g ~ 3.2 eV), rendering it less efficient for its use in solar photocatalysis^(1,6,9).

Moreover, the enhanced photocatalytic activity can be attributed to the synergetic effect of morphology, crystallinity, and surface area of the TiO₂ and these features can be effectively tuned controlling the synthesis conditions of the nanostructures⁽¹⁵⁾. Recently, Quintero et. al.,⁽¹⁴⁾ reported that the properties of the synthesized TiO₂ nanostructures by sol-gel technique

strongly-depend on the synthesis route and their processing condition (reagent concentration, pH, acid catalysts, stirring time and calcination temperature). To prepare TiO₂ nanoparticles with excellent adsorption performance through an eco-friendly route, several methods have been applied to improve the photocatalytic efficiency of TiO₂^(4, 9-16). Therefore, it has been reported that the synthesis methods have an important effect on the morphology, homogeneity, and photocatalytic activity of metal oxide semiconductors^(1,16-19).

Thus, the aim of this study is to synthesize nanoparticles of TiO₂ at different temperatures by an easy and reproducible preparation route. The synthesis by sol-gel technique has been one of the most promising methods to prepare nanostructured powders with interesting properties, due to its simplicity and low production costs⁽¹⁴⁾.

Additionally, the incorporation of ultrasound in several chemical synthesis has been an effective process to reduce the particle size of nano powders^(14,20,21). Also, is a process used to disperse the ions and nanoparticles into the polymer matrix. However, in this research, an ultrasonic-assisted sol-gel method is employed to obtain TiO₂ nanoparticles with reduced particle size and their structural and optical properties investigated. A quantum size effect (QSE) is considered to explain the blue shift, which could be the cause of the enhancing in the photodegradation of methyl orange (MO) in the visible light spectral region.

2. Methodology

2.1. Materials

For the synthesis of pure TiO₂, titanium tetra isopropoxide (TTIP, supplied by Sigma-Aldrich with purity of 97 %) and acetic acid (purity of 100 % supplied by Emsure) were used without further purification. For the photocatalytic reaction tests, methyl orange (MO, with purity ≥ 97 %) dye was purchased from Sigma-Aldrich. All the aqueous

solution was prepared using distilled and deionized water.

2.2. Synthesis of TiO₂ nanoparticles

In this work, 5 mL of acetic acid was dissolved in 250 mL of distilled and deionized water in a beaker. The mixed solution was used as the hydrolysis catalyst. Then, 5 mL of the TTIP precursor was placed in a syringe and instantly added to the above solution. Immediately, the resulting solution was sonicated at 70 °C for 3 h and then dried in a hotplate at 70 °C for about 36 h. After that, the dried sol-gel product was pulverized with mortar to obtain a fine powder for analysis. The finely pulverized sample was subjected to a heat treatment in a muffle furnace at 400, 450 and 500 °C for 3 h. A yellow-white powder was obtained. The present method used for the synthesis of TiO₂ nanoparticles was described by Quintero et al. ⁽¹⁴⁾ with different conditions of synthesis.

2.3. Characterization

XRD analyses were carried out in a Bruker D8 Advance diffractometer with CuK_{α1} radiation ($\lambda = 0.154\text{nm}$) at room temperature (RT). The XRD was operated at 40 kV and 30 mA, with scanning angle range of 20-80° and increment of 0.02°, respectively. A FTIR spectrophotometer (IRAffinity-1S, Shimadzu) was used to obtain the IR spectra of the samples using the KBr method. A Jeol/JSM-6490 scanning electron microscope (SEM) operated at 20 kV, equipped with an energy dispersive X-ray (EDX) detector was used for compositional analyses. A Tecnai F20 FEG-S/TEM operated at 200 kV was used to characterize the samples. Absorbance measurements was analyzed using a Chromtech spectrophotometer CT-8600. Photoluminescence (PL) measurements were performed at RT in a Jasco Spectrofluorometer FP-8500. The concentration of MO solutions was analyzed

using a Rayleigh UV-Visible Spectrophotometer, UV1800.

2.4. Test of MO degradation

The photocatalytic activity was carried out in a batch reactor using an Illuminator LuzChem LZC-4V photoreactor equipped with 14 lamps (Sylvania F13T8 13W, Cool White, 412 K Color Temperature) with emission in the visible range, from 400 to 700 nm. The energy density of the light irradiation on the surface of the sample was 4.5 J/cm², as measured with a UVX radiometer under continuous illumination. The synthesized samples were used as a catalyst for the degradation of MO solution. Without the presence of the catalyst, the MO was first tested to observe its stability.

Reaction mixtures were prepared by adding 1g/L of photocatalyst into MO solution (5 ppm). The mixture (MO solution and nanoparticles) was kept in stirring and darkness for 1 hour until adsorption equilibrium was achieved. The photoreactor was irradiated under continuous shaking, and samples from the suspension were collected at regular time intervals, centrifuged, and filtered. The MO concentration in solution was measured through a calibration curve of the absorbance at 465 nm using a UV-visible spectrophotometer, which is the maximum absorption of MO. The results were corrected for the decomposition of the MO dye in the absence of a photocatalyst. The Eq. 1 was used to determine the degradation efficiencies of MO dye,

$$\eta = \left[1 - \frac{C}{C_0}\right] * 100 \quad (1)$$

where, C_0 and C are the concentrations of the solution at $t = 0$ and t minutes under visible light.

3. Results and discussion

Figure 1 shows XRD patterns of the synthesized TiO₂ nanoparticles (NPs) and calcined at 400, 450, and 500 °C. The prepared TiO₂ NPs crystallize in the anatase structure (JCPDS 89-4921)⁽¹⁾ with diffraction peaks located at 2θ values and Miller's indexes (101), (004), (200), (105), (211), (204), (116), (220) and (215), respectively. This indicates that no relevant changes were obtained in their crystalline structure due to the calcination during the preparation of these photocatalysts. Therefore, the formation of anatase TiO₂ nanoparticles can be confirmed.

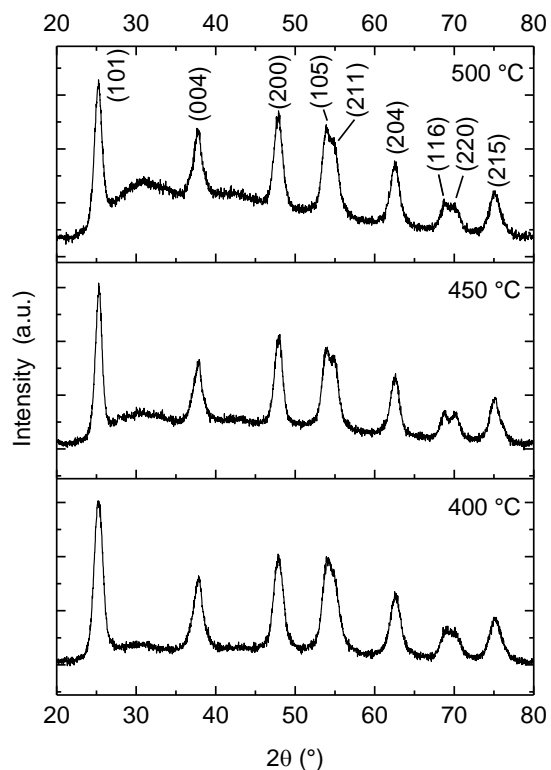


Figure 1. XRD patterns of TiO₂ nanoparticles calcined at: (a) 400 °C (b) 450 °C, and (c) 500 °C.

In addition, XRD can be used to determine the crystallite size which was calculated by the x-ray line broadening method employing the average of the three principal peaks at (101), (004) and (200), using the Scherrer formula (Eq. 2)^(3,22-24):

$$D = \frac{k\lambda}{\beta \cos\theta} \quad (2)$$

where D is the crystalline size, k is the shape factor (0.9 for spherical particles⁽²⁵⁾) and assumed the peak to be Gaussian, λ is the wavelength of CuK α source (0.15405 nm), and β is the full width at half maximum (FWHM) of each the diffraction peaks. The TiO₂ crystallite sizes varied each other according to XRD patterns when the synthesis temperature is changed. The crystallite size is reported in Table 1. Further, the smaller sized TiO₂ nanoparticles here reported possess a similar crystallite size to the anatase phase without calcination from a previous work⁽¹⁴⁾. Instead, for the samples calcined at 450 and 500 °C, the crystallite size increased.

Figure 2 shows the energy dispersive X-ray spectroscopy (EDX), which indicates that the elements Ti, and O are present in the samples (the presence of Al is due to the sample holder). No other impurities are observed, indicating the high quality of the product. The morphology (size and shape) of the NPs was investigated with TEM technique (Figure 3). In all samples there is agglomeration of nanoparticles which are spherical shape. The typical micrographs consist of agglomerated TiO₂ nanoparticles with an average diameter less than 15 ± 2 nm, which is slightly larger than the crystallite size calculated by Scherrer's formula (see Table 1) from XRD analysis. Therefore, XRD analysis is used to estimate the crystallite size in a nanocrystal while TEM micrographs are used to determine the particle size^(14,21). In addition, increasing the calcinated temperature will favors an increase in the nanoparticle size or promote change in the crystalline phase.

An FTIR was used to determine the functional groups of the samples. The vibrational frequencies have been recorded in the range of 4000–500 cm⁻¹ (Figure 4a). The bands present at ~ 3330 and 1635 cm⁻¹ is due to the stretching vibrations of O–H groups and to the H–O–H bending vibrations of adsorbed water. In

addition, peaks around 1000 and 500 cm^{-1} are related to the metal-oxygen stretching mode in the TiO_2 lattice.

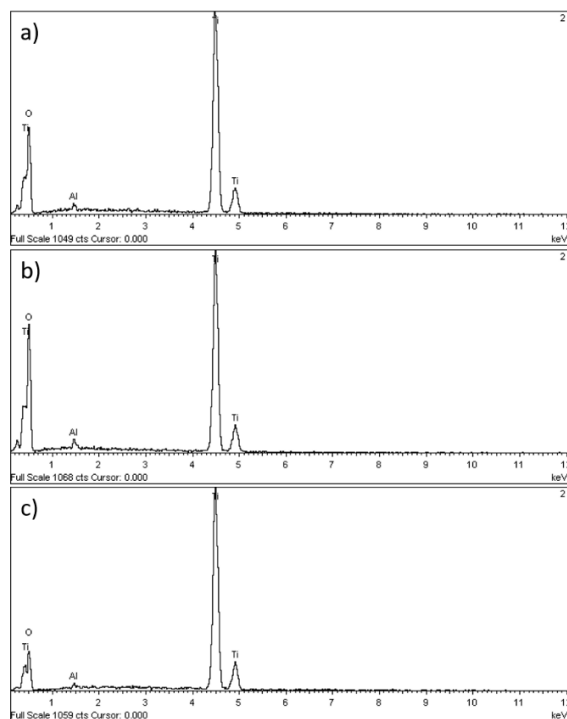


Figure 2. Compositional analysis of TiO_2 nanoparticles calcined at: (a) 400 °C (b) 450 °C, and (c) 500 °C.

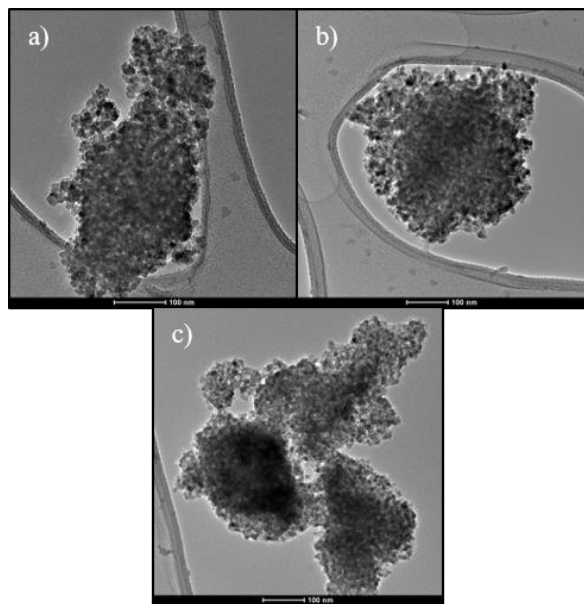


Figure 3. TEM images of samples calcined at: (a) 400 °C (b) 450 °C, and (c) 500 °C.

UV-vis absorbance and photoluminescence (PL) studies performed at room temperature (RT), have been employed to examine the optical properties of the samples. Here, we observed that the optical absorption edge exhibits a blue shift ($\Delta E_g = 0.49 \pm 0.10$ eV) with respect to the bulk (Anatase phase, 387 nm, $E_g \sim 3.2$ eV^(1,2,10,19)).

The optical band gap of the samples, Fig. 4b-d, was determined based on the dependence of the absorption coefficient (α) and the photon energy ($h\nu$). For direct transitions, the corresponding band gap energy (E_g) were estimated through Tauc's plot^(1,11,27) ($(\alpha h\nu)^2$ versus $h\nu$ plot to $\alpha = 0$). It is observed that the E_g of the samples increases with respect to the synthesis temperature showing a blue shift, which could be explained by the quantum size effect (QSE) of TiO_2 nanocrystals, see Table 1.

However, a photocatalyst with the large E_g will have a better performance in the near-solar UV region. But the observed results demonstrate that TiO_2 anatase nanocrystals will be prospective visible light active photocatalysts even if their E_g is considerably larger than the bulk (anatase phase) as reported by Vorontsov and Valdés⁽²⁷⁾.

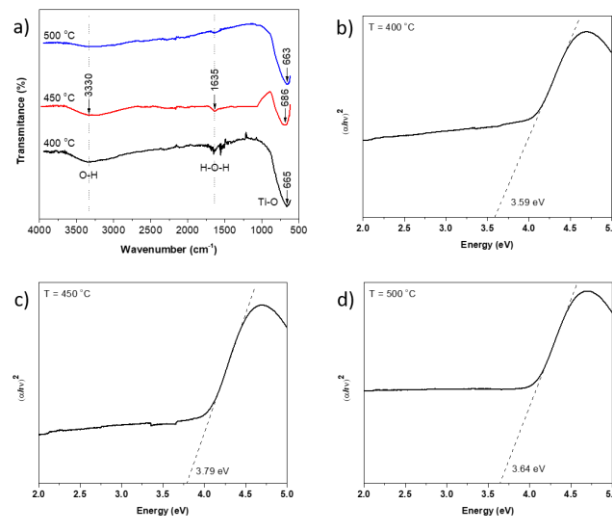


Figure 4. (a) Infrared spectra and (b-d) energy band gap of the calcined samples.

Room temperature photoluminescence (PL) spectra were recorded for further analysis of the electron-hole recombination process of the samples (see Figure 5 a-c). The samples were excited using light of wavelengths at 254, 312, and 365 nm, respectively. No change was observed both in the shape and emission peaks in the PL spectra of all samples tested. The peak observed around 342 nm (3.63 eV) corresponds to the band-edge emission of the TiO₂ nanocrystals⁽¹⁾.

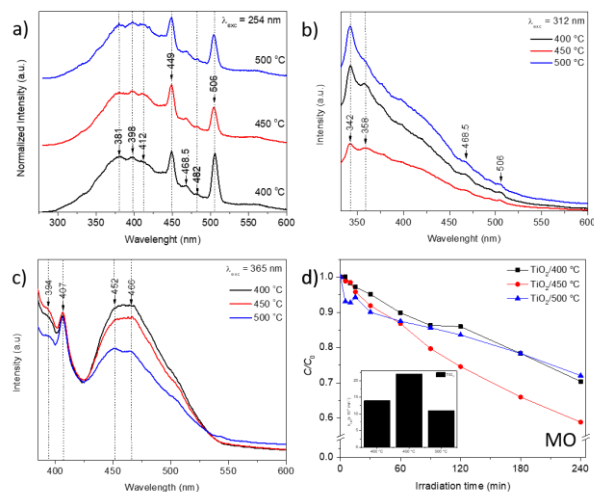


Figure 5. RT-PL spectra of samples excited at (a) 254 nm, (b) 312 nm, and (c) 365nm. (d) Photocatalytic activity of synthesized photocatalysts. The inset shows the plot of the observed degradation rate constant of MO for different samples under visible light irradiation.

This result match very well with obtained by UV-vis and is in agrees with the reported values of electronic band gap and optical band gap obtained by Vorontsov and Valdés⁽²⁷⁾. Instead, the TiO₂ absorption edge is characteristic of an UV material. In addition, the origin of the violet-blue emission observed in PL measurements could be ascribed to shallow trap levels induced by the presence of oxygen vacancies (Vo)⁽²⁸⁻³¹⁾. Romero Sáez et. al,⁽¹⁾ reported that in pure TiO₂, the PL emission is attributed to oxygen vacancies (Vo), which was confirmed by XPS

measurements⁽³²⁻³⁵⁾. In addition, Romero Sáez et al,⁽¹⁾ and Saravanan et al,⁽¹⁰⁾ reported that incorporation of carbon (C) and chitosan (CS) in the TiO₂ structure increase the photocatalytic activity of TiO₂ nanoparticles in the visible region.

The synthesized TiO₂ NPs have been examined as a photocatalyst for the photodegradation of MO. Figure 5d displays the MO degradation curves versus irradiation time for all samples. The degradation of MO dye under visible light and its efficiency are determined from Eq. (1) and the calculated values are reported in Table 1.

Table 1. Crystallite size and bandgap values, along with the degradation efficiency of all samples under visible light irradiation.

Sample	Crystallite size, D, (nm)	Band gap (eV)	Degradation efficiency (MO dye, 60 min, visible light) (%)	Degradation efficiency (MO dye, 240 min, visible light) (%)
400 °C	7.1	3.59	10.2	29.6
450 °C	9.1	3.79	13.2	41.1
500 °C	8.6	3.64	12.5	27.9

After 240 min of samples illumination, the results showed how the MO concentration decreased with irradiation time (less than 50 %). The maximum efficiency is achieved for the sample calcined at 450 °C, which shows 41.1 % efficiency, followed by 29.6 % (at 400 °C) and 27.9 % (at 500 °C). Therefore, the photocatalytic performance of the samples is attributed to the structural and optical characteristics of the material. In addition, extending the absorption spectrum to the visible light region provide opportunities of designing advanced photocatalytic materials.

On the other hand, the photocatalytic first order rate constant (*k*) was calculated using the Eq. 3

$$k = \ln\left(\frac{C}{C_0}\right)/t \quad (3)$$

which was reported by Gnanasekaran et al.⁽¹⁹⁾. Here, it is also found that the observed degradation rate (k) for sample calcined at 450 °C is higher than those calcined at 400 and 500 °C (Figure 5d, inset). Therefore, the results show that the photocatalytic activity of TiO₂ nanocrystals mainly depends on the synthesis method, crystallinity, morphology, the energy gap and lattice defects^(1,3-19).

4. Conclusions

In summary, TiO₂ NPs were successfully synthesized employing an ultrasonic-assisted sol gel method. The TiO₂ NPs crystallize in the anatase structure with a highly crystalline order. Based on the quantum size effect (QSE), the optical properties show that the absorption and emission peaks are blue shifted in comparison to the bulk. In addition, the optical band gap was found to be 3.69 ± 0.10 eV for crystallites size less than 10 nm. PL analysis showed that oxygen vacancies were generated in all samples, which can also cause absorption and reaction under visible light, enhancing the photocatalytic activity of the nanomaterial prepared. All samples were photoactive for MO degradation after 240 min of being irradiated with visible light. The best performing TiO₂ nanocrystals we obtained, according to their degradation efficiency on MO, correspond to those calcined at 450 °C. The results provide new insights about the synthesis of TiO₂-based photocatalysts with notable visible light activity for interesting and potential environmental applications.

5. Conflict of interest

The authors declare that they have no conflict of interest.

6. Acknowledgements and Funding Statement

The authors acknowledge the support of Universidad del Valle through the projects C.I.

71152, C.I 71154, and “Apoyo al Fortalecimiento de os Centros e Institutos – VRP”. In addition, thanks to Y. Quintero and Dr. A. García from Advanced Mining Technology Center, Universidad de Chile – Chile, for photocatalytic measurements.

7. References

- (1) Romero-Sáez M, Jaramillo L Y, Saravanan R, Benito N, Pabón E, Mosquera E, Gracia F. Notable photocatalytic activity of TiO₂-polyethylene nanocomposites for visible light degradation of organic pollutants. *eXPRESS Polym. Lett.* 2017; 11:899–909. <http://doi.org/10.3144/expresspolymlett.2017.86>
- (2) Mehrabi M, Javanbakht V. Photocatalytic degradation of cationic and anionic dyes by removal a novel nanophotocatalyst of TiO₂/ZnTiO₃/α-Fe₂O₃ by ultraviolet light irradiation. *J Mater. Sci: Mater. Electron.* 2018; 29:9908–9919. <https://doi.org/10.1007/s10854-018-9033-0>
- (3) Lassoued A, Lassoued M S, Dkhil B, Ammar S, Gadri A. Photocatalytic degradation of methyl orange dye by NiFe₂O₄ nanoparticles under visible irradiation: effect of varying the synthesis temperature. *J Mater. Sci: Mater. Electron.* 2018; 29(9):7057–7067. <https://doi.org/10.1007/s10854-018-8693-0>
- (4) Khan M M, Ansari S A, Pradhan D, Ansari M O, Han D H, Lee J, Cho M H. Band gap engineered TiO₂ nanoparticles for visible light induced photoelectrochemical and photocatalytic studies. *J. Mater. Chem. A.* 2014; 2:637–644. <https://doi.org/10.1039/C3TA14052K>

- (5) Saravanan R, Sacari E, Gracia F, Khan M M, Mosquera E, Gupta V K. Conducting PANI stimulated ZnO system for visible light photocatalytic degradation of coloured dyes. *J. Mol. Liquids*. 2016; 221:1029–1033.
<https://doi.org/10.1016/j.molliq.2016.06.074>
- (6) Khan M M, Ansari S A, Amal M I, Lee J, Cho M H. Highly visible light active Ag@TiO₂ nanocomposites synthesized using an electrochemically active biofilm: a novel biogenic approach. *Nanoscale*. 2013; 5:4427–4435.
<https://doi.org/10.1039/C3NR00613A>
- (7) Khan M M, Lee J, Cho M H. Au@TiO₂ nanocomposites for the catalytic degradation of methyl orange and methylene blue: An electron relay effect. *Journal of Industrial and Engineering Chemistry*. 2014; 20:1584–1590.
<https://doi.org/10.1016/j.jiec.2013.08.002>
- (8) Yuan J, Zhang X, Li H, Wang K, Gao S, Yin S, Yu H, Zhu X, Xiong Z, Xie Y. TiO₂/SnO₂ double-shelled hollow spheres-highly efficient photocatalyst for the degradation of rhodamine B. *Catalysis Communications*. 2015; 60:129–133.
<https://doi.org/10.1016/j.catcom.2014.11.032>
- (9) Kalathil S, Khan M M, Ansari S A, Lee J, Cho M H. Band gap narrowing of titanium dioxide (TiO₂) nanocrystals by electrochemically active biofilms and their visible light activity. *Nanoscale*. 2013; 5:6323–6326.
<https://doi.org/10.1039/c3nr01280h>
- (10) Saravanan R, Aviles J, Gracia F, Mosquera E, Gupta V K. Crystallinity and lowering band gap induced visible light photocatalytic activity of TiO₂/CS (Chitosan) nanocomposites. *Int. J. Biol. Macromol.* 2018; 109:1239–1245.
<https://doi.org/10.1016/j.ijbiomac.2017.11.125>
- (11) Kanna M, Wongnawa S. Mixed amorphous and nanocrystalline TiO₂ powders prepared by sol-gel method: Characterization and photocatalytic study. *Mater. Chem. Phys.* 2008; 110:166–175.
<https://doi.org/10.1016/j.matchemphys.2008.01.037>
- (12) Imran M, Riaz S, Naseem S. Synthesis and characterization of titania nanoparticles by sol-gel technique. *Mater. Today*. 2015; 2(10):5455–5461.
<https://doi.org/10.1016/j.matpr.2015.11.069>
- (13) Dubey R. Temperature-dependent phase transformation of TiO₂ nanoparticles synthesized by sol-gel method. *Mater. Lett.* 2018; 215:312–317.
<https://doi.org/10.1016/j.matlet.2017.12.120>
- (14) Quintero Y, Mosquera E, Diosa J, García A. Ultrasonic-assisted sol-gel synthesis of TiO₂ nanostructures: Influence of synthesis parameters on morphology, crystallinity, and photocatalytic performance. *J Sol-Gel Sci. Technol.* 2020; 94:477–485
<https://doi.org/10.1007/s10971-020-05263-6>
- (15) García A, Quintero Y, Vicencio N, Rodríguez B, Ozturk D, Mosquera E, Corrales T P, Volkmann U G. Influence of TiO₂ nanostructures on anti-adhesion and photoinduced bactericidal properties of thin film composite membranes. *RSC Adv.* 2016;

- 6:82941–82948.
<https://doi.org/10.1039/C6RA17999A>
- (16) Wang C L, Hwang W S, Chu H L, Lin H J, Ko H H, Wang M C. Kinetic of anatase transition to rutile TiO₂ from titanium dioxide precursor powders synthesized by a sol-gel process. *Ceram. Inter.* 2016; 42:13136–13143.
<https://doi.org/10.1016/j.ceramint.2016.05.101>
- (17) Rajendran S, Khan M M, Gracia F, Qin F, Gupta V K, Arumainathan S. Ce³⁺-ion-induced visible-light photocatalytic degradation and electrochemical activity of ZnO/CeO₂ nanocomposite. *Sci. Rep.* 2016; 6:31641.
<https://doi.org/10.1038/srep31641>
- (18) Saravanan R, Gupta V K, Mosquera E, Gracia F. Preparation and characterization of V₂O₅/ZnO nanocomposite system for photocatalytic application. *J. Mol. Liquids.* 2014; 198:409–412.
<https://doi.org/10.1016/j.molliq.2014.07.030>
- (19) Gnanasekaran L, Hemamalini R, Saravanan R, Ravishandran K, Gracia F, Gupta V K. Intermediate state created by dopant ions (Mn, Co, and Zr) into TiO₂ nanoparticles for degradation of dyes under visible light. *J. Mol. Liquids.* 2016; 223:652–659.
<https://doi.org/10.1016/j.molliq.2016.08.105>
- (20) Karthik K, Nikolova M P, Phuruangrat A, Pushpa S, Revathi V, Subbulakshmi M. Ultrasonic-assisted synthesis of V₂O₅ nanoparticles for photocatalytic and antibacterial studies. *Mater. Res. Innov.* 2020; 24(4): 229–234.
<https://doi.org/10.1080/14328917.2019.1634404>
- (21) Wong C W, Chan Y S, Jeevanandam J, Pal K, Bechelany M, Elkodous M A, El-Sayyad G S. Response surface methodology optimization of mono-disperse MgO nanoparticles fabricated by ultrasonic-assisted sol-gel method for outstanding antimicrobial and antibiofilm activities. *J. Cluster Sci.* 2020; 31:367–389.
<https://doi.org/10.1007/s10876-019-01651-3>
- (22) B. D. Cullity. *Elements of X-Ray Diffraction.* Addison Wesley, 2nd Ed. 1978.
- (23) Zak A K, Majid W H A, Abrishami M E, Yousefi R. X-ray analysis of ZnO nanoparticles by Williamson-Hall and size-strain plot methods. *Solid State Sci.* 2011; 13:251–256.
<https://doi.org/10.1016/j.solidstatesciences.2010.11.024>
- (24) Mosquera E, Rojas-Michea C, Morel M, Gracia F, Fuenzalida V, Zárata R A. Zinc oxide nanoparticles with incorporated silver: Structural, morphological, optical and vibrational properties. *Appl. Surf. Sci.* 2015; 347:561–568.
<https://doi.org/10.1016/j.apsusc.2015.04.148>
- (25) Patterson A L. The Scherrer formula for X-ray particle size determination. *Phys. Rev.* 1939; 56:978–982.
<https://doi.org/10.1103/PhysRev.56.978>
- (26) Viezbicke B D, Patel S, Davis B E, Birnie D P. Evaluation of the Tauc method for optical absorption edge determination:

- ZnO thin films as a model system. *Physica Status Solidi B*. 2015; 252:1700–1710. <https://doi.org/10.1002/pssb.201552007>
- (27) Vorontsov A V, Valdés H. Quantum size effect and visible light activity of anatase nanosheet quantum dots. *J. Photochem Photobiol. A: Chem.* 2019; 379:39–46. <https://doi.org/10.1016/j.jphotochem.2019.05.001>
- (28) Morgan B J, Watson G W. Intrinsic n-type defect formation in TiO₂: A comparison of rutile and anatase from GGA+U calculations. *J. Phys. Chem. C*. 2010; 114: 2321–2328. <https://doi.org/10.1021/jp9088047>
- (29) Tshabalala Z P, Motaung D E, Mhlongo G H, Ntwaeaborwa O M. Facile synthesis of improved room temperature gas sensing properties of TiO₂ nanostructures: Effect of acid treatment. *Sens. Actuators B: Chem.* 2016; 224:841–856. <https://doi.org/10.1016/j.snb.2015.10.079>
- (30) Santara B, Giri P K, Imakita K, Fujii M. Evidence for Ti interstitial induced extended visible absorption and near infrared photoluminescence from undoped TiO₂ nanoribbons: An in situ photoluminescence study. *J. Phys. Chem. C*. 2013; 117:23402–23411. <https://doi.org/10.1021/jp408249q>
- (31) Tachikawa T, Majima T. Single-molecule, single-particle fluorescence imaging of TiO₂-based photocatalytic reactions. *Chem. Soc. Rev.* 2010; 39:4802–4819. <https://doi.org/10.1039/B919698F>
- (32) Benito N, Palacio P. Growth of Ti–O–Si mixed oxides by reactive ion-beam mixing of Ti/Si interfaces. *J. Phys. D: Appl. Phys.* 2014; 47:015308/1–7. <https://doi.org/10.1088/0022-3727/47/1/015308>
- (33) Luan Z, Maes E M, van der Heide P A W, Zhao D, Czernuszewicz R S, Kevan L. Incorporation of titanium into mesoporous silica molecular sieve SBA-15. *Chem. Mater.* 1999; 11:3680–3686. <https://doi.org/10.1021/cm9905141>
- (34) Suzana M, Francisco P, Mastelaro V R, Nascente P A P, Florentino A O. Activity and characterization by XPS, HR-TEM, Raman spectroscopy, and BET surface area of CuO/CeO₂-TiO₂ catalysts. *J. Phys. Chem. B*. 2001; 105:10515–10522. <https://doi.org/10.1021/jp0109675>
- (35) Li Y, Hwang D S, Lee N H, Kim S J. Synthesis and characterization of carbon-doped titania as an artificial solar light sensitive photocatalyst. *Chem. Phys. Lett.* 2005;404:25–29. <https://doi.org/10.1016/j.cplett.2005.01.062>